Phenomenological $pn \rightarrow pp\pi^-$ model of $A(p,\pi^-)B$ reactions

W. R. Falk*
Department of Physics and Astronomy, University of Manitoba, Winnipeg, Manitoba, Canada, R3T 2N2

S. Karataglidis†
Department of Physics, University of Johannesburg, P.O. Box 524, Auckland Park 2006, South Africa
(Received 30 January 2012; revised manuscript received 4 June 2012; published 14 December 2012)

A phenomenological $pn \rightarrow pp\pi^-$ model of $A(p,\pi^-)B$ reactions is developed that incorporates the spin dependence of the former reaction. The model development follows closely that of the $pp \rightarrow d\pi^+$ model for $A(p,\pi^+)C$ reactions. Predictions of the analyzing powers and differential cross sections for the (p,π^-) reaction on ^{13}C at 200 MeV are presented and discussed. Calculated differential cross sections describe reasonably well the shape of the experimental data, although the predicted strengths vary considerably. Model predictions of the analyzing powers are in general agreement with the data. Nuclear structure amplitudes are obtained from a no-core multi-$\hbar\omega$ shell model. Sensitivities of the observables to the nuclear structure details and also the amplitudes of the primary $pn \rightarrow pp\pi^-$ reaction are investigated.

DOI: 10.1103/PhysRevC.86.064606 PACS number(s): 25.40.Qa, 24.10.−i, 21.45.−v, 24.70.+s

I. INTRODUCTION

Nuclear pion production induced by protons of a few hundred MeV has been shown to proceed primarily via the two-nucleon mechanism $NN \rightarrow NN\pi$. Detailed comparative studies [1] of $(p,\pi^\pm)$ on ^{13}C have shown that the selectivity of these reactions are consistent with this picture for both π^+ and π^- production. In particular, the two-nucleon mechanism is able to qualitatively explain the selectivity for exciting high-spin two-particle, one-hole states in the (p,π^-) reaction. A discussion and review of earlier work on the (p,π^-) reaction is given by Korkmaz *et al.* [1]. Confirming evidence for the $NN \rightarrow NN\pi$ production mode in nuclei has been demonstrated in the case of the (p,π^+) reaction in the context of a $pp \rightarrow d\pi^+$ model [2]. This model was applied to a range of nuclear targets and bombarding energies of 200–500 MeV, as well as to the calculation of various observables in the near-threshold $pd \rightarrow {}^3\mathrm{H}\pi^+$ and $pd \rightarrow {}^3\mathrm{He}\pi^0$ reactions [3].

In this paper we discuss the development of a parallel model that incorporates as input the experimental data for the $\vec{p}n \rightarrow pp\pi^-$ reaction [4–8]. This model is used in the calculation of observables for π^- production on nuclei. An extensive set of measurements of the differential cross sections and analyzing powers exists for the $^{13}\mathrm{C}(\vec{p},\pi^-)^{14}\mathrm{O}$ reaction [1] and, to a lesser extent, for the targets of ^{12}C and ^{14}C [9]; the model is applied to the former. The availability of differential cross-section and analyzing power data for numerous final states in the same nucleus is important in the testing of the model, as this affords the opportunity to examine the sensitivity to nuclear structure details, angular momentum effects, etc., for the same incident channel.

The experimental angular distributions of the analyzing powers and differential cross sections of nuclear pion production show distinctly different π^+ and π^- characteristics [1]. First, the analyzing powers for π^+ production are largely negative and rather similar to those of the $pp \rightarrow d\pi^+$ reaction. For π^- production, on the other hand, the analyzing powers are typically positive in the angular range 45° to 90°. The differential cross sections for π^+ are much greater in magnitude than those for π^- production. They also differ in shape: the latter's angular distributions are typically quite flat and featureless, while those for π^+ drop rapidly with increasing angle and often have a deep minimum. Comparing differential cross-section magnitudes at forward angles for pion production on ^{13}C at 200 MeV, one finds ∼300 nb/sr for π^+ and ∼4 nb/sr for π^-, or a ratio of 75 between them. These are the general features and many exceptions can be found in the published data. Any model of $\pi^\pm$ production must be able to account for these differences.

Theoretical investigations of $A(p,\pi^-)B$ reactions in a two-nucleon model have been reported in a series of papers by Kume and collaborators [10]. Their calculations [11,12] show a pronounced selectivity for exciting high-spin stretched 2p-1h states in reactions on medium-mass nuclei ^{48}Ca and ^{88}Sr. Spectra for (p,π^-) reactions on Ca isotopes are reasonably well reproduced [12]. They conclude that the final $pp(^1S_0)$ channel [11] dominates the two-body $pn \rightarrow pp\pi^-$ process. However, the $pp(^3P)$ channel also makes a contribution and interferes with the $pp(^1S_0)$ channel. Their calculations for the (p,π^-) reaction on the carbon isotopes are limited to the ground-state transitions for the targets ^{12,14}C. The situation here is considerably more complicated because of the large angular momentum mismatch. They find that the analyzing powers are strongly influenced by pion distortion effects [13], while core polarization affects mainly the magnitude of the cross sections [14].

Table I lists the possible proton-induced $NN \rightarrow NN\pi$ cross sections, classified according to the isospin of the initial (I) and final (I') NN states. Production of π^+ and π^0 involves all $\sigma_{II'}$ cross sections, whereas π^- production involves only σ_{11} and σ_{01}. Consequently, while many partial waves contribute to each

*falk@physics.umanitoba.ca
†stevenka@uj.ac.za

TABLE I. $NN \to NN\pi$ isospin cross sections $\sigma_{II'}$.

$NN \to NN\pi$	σ_{10}^{d}	σ_{10}	σ_{11}	σ_{01}
$pp \to d\pi^+$	1			
$pp \to pn\pi^+$		1	1	
$pn \to nn\pi^+$			$\frac{1}{2}$	$\frac{1}{2}$
$pn \to d\pi^0$	$\frac{1}{2}$			
$pn \to pn\pi^0$		$\frac{1}{2}$		$\frac{1}{2}$
$pp \to pp\pi^0$			1	
$pn \to pp\pi^-$			$\frac{1}{2}$	$\frac{1}{2}$

of these cross sections, π^- production should be somewhat simpler in its description. Furthermore, it can be argued that, because of angular momentum effects, only a small subset of the partial waves in σ_{11} and σ_{01} will be important in nuclear π^- production at low energies. At bombarding energies up to 500 MeV the σ_{10}^{d} and σ_{10} cross sections are much greater than the σ_{11} and σ_{01} cross sections. At the fundamental $NN \to NN\pi$ level this may be attributed to the well-known dominance of pion p-wave production over that for s-wave production for π^+ and π^-, respectively. It is quite understandable, then, that nuclear π^+ production would be much stronger than π^- production.

Because (p,π^+), and presumably (p,π^0), cross sections are much larger than those for (p,π^-), a process that may be important to π^- production on nuclei is pion charge exchange. The role of (p,π^0) production, forming the isobaric analog of the (p,π^-) final state, followed by single charge exchange, needs to be investigated but is beyond the scope of this paper.

II. $pn \to pp\pi^-$ MODEL

A. Relation to $pp \to d\pi^+$ model

The model for (p,π^+) reactions is described in detail in Ref. [2]. Here only a brief overview of this model is given, as required to understand the ingredients of the (p,π^-) model. Thereafter the modifications and extensions of the earlier model, appropriate for (p,π^-) reactions, are outlined. For practical reasons of making the many sums and integrals of the phenomenological model tractable, certain compromises were necessitated. One of these was the use of an harmonic oscillator basis for the expansion of the final nucleus wave function in terms of a core plus two protons as described in Ref. [2].

The $pp \to d\pi^+$ model for $A(p,\pi^+)C$ incorporates the following essential features:

(i) Two-step process. An incident proton with momentum $\mathbf{k}_p$ [in the $(p+A)$ center-of-mass (c.m.) system] interacts with a target proton of momentum $(\mathbf{k}_0)$, producing a pion of momentum $\mathbf{k}_\pi$ and an associated deuteron. The deuteron ($^3S_1$) recombines with the recoil nucleus to form the final nucleus C. The intermediate nucleus (the target with the struck proton removed) is referred to as the core.

(ii) Momentum sharing. In a plane-wave representation, the relative momentum $\mathbf{q}$ of this deuteron with respect to the recoil nucleus is given by

$$\mathbf{q} = \left(\frac{A-1}{A}\right)\mathbf{k}_p + \mathbf{k}_0 - \left(\frac{A-1}{A+1}\right)\mathbf{k}_\pi. \quad (1)$$

(iii) On-shell amplitudes for $pp \to d\pi^+$.

(iv) The pion momentum in the $A(p,\pi^+)B$ reaction defines the momentum at which the on-shell $pp \to d\pi^+$ amplitudes are evaluated.

(v) Angular quantities, however, are determined by the $pp \to d\pi^+$ reaction in it c.m. frame.

(vi) Plane waves for protons and pions, with distortions treated through Eikonal approxmations.

(vii) Full angular momentum and isospin couplings.

(viii) Nuclear structure amplitudes from nuclear wave functions.

The $pn \to pp\pi^-$ model for $A(p,\pi^-)B$ reactions requires the following modifications:

(i) The target nucleon is a neutron rather than a proton.

(ii) Recaptured nucleons are two protons in the $^1S_0$ or $^3P_0$, $T=1$ state, rather than a deuteron ($^3S_1$, $T=0$). (Justification is given for subsuming other ^3P configurations into $^3P_0$.)

(iii) Effective amplitudes for the $pn \to pp\pi^-$ reaction from experiment, as described in Sec. II C.

B. Relative motion pp wave function

In the $pp \to d\pi^+$ model for (p,π^+) reactions the internal pn wave function $\psi(r)$ was effectively replaced by the deuteron internal wave function via the expression

$$\left[\frac{\psi(r)}{\psi_d(r)}\right]_{r=a}\psi_d(\mathbf{r}). \quad (2)$$

This form was used as $\psi_d(\mathbf{r})$ is required in the $pp \to d\pi^+$ matrix element. Likewise, in the (p,π^-) reaction the wave function $\psi_{pp}(\mathbf{r})$ is required in the $pn \to pp\pi^-$ matrix element. The normalizing factor, $\psi(r)$ divided by $\psi_{pp}(r)$, is applied as shown in Eq. (3):

$$\frac{\left|\int \psi(r)dr\right|}{\left|\int \psi_{pp}(r)dr\right|}\psi_{pp}(\mathbf{r}). \quad (3)$$

Here $\psi(r)$ is the internal pp wave function of the recaptured protons in the final nucleus. It is conveniently expressed via harmonic oscillator functions $H_{n,l=0}$ and $H_{n,l=1}$, given the expansion of the nucleus in these functions. For $\psi_{pp}(r)$ the free low-energy pp scattering wave functions for $^1S_0$ and $^3P_0$ are used.

The scattering wave functions are described in the paper by Loiseau and Mathelitsch [15]. They are shown in Fig. 1 at 4 MeV c.m. by the solid lines. Also shown are the corresponding functions H_{nl}. This choice of 4 MeV is arbitrary, as an averaging over energy was carried out. The scattering wave functions have the asymptotic behavior

$$\psi_{pp}(r) = \sin(kr + \delta(k))/kr, \quad (4)$$

while the harmonic oscillator functions have the normalization $\int H_{nl}^2 r^2 dr = 1$.

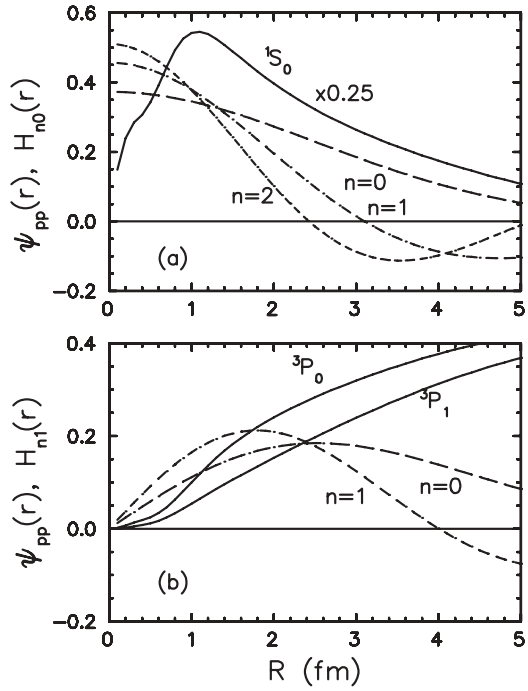

FIG. 1. The pp scattering wave functions at 4 MeV c.m. (solid lines) and harmonic oscillator functions (dashed lines) for (a) $^1S_0$ and (b) $^3P_0$ and $^3P_1$.

The functions shown in the above figure were integrated between $0 \leqslant r \leqslant R$ to obtain the ratio

$$\frac{\left|\int H_{nl}(r)dr\right|}{\left|\int \psi_{pp}(r)dr\right|}. \tag{5}$$

Because this ratio is a complicated function of both energy and R some approximations had to be made, and these were handled as follows. For an upper integration limit in the neighborhood of $R = 2$ fm, this ratio changes quite slowly as a function of R and has the same values for $n = 0, 1, 2$ for $^1S_0$. Although the ratios for $^3P_0$ and $^3P_1$ do not vary as slowly as a function of R, the value of $R = 2$ fm was, somewhat arbitrarily, adopted for both. In the final analysis an improper evaluation of this overlap integral will be reflected in modified values for the partial wave amplitudes, as discussed in the following section.

In order to take into account the energy dependence of these ratios it is to be noted that at low energies the scattering wave functions have roughly a constant shape and only their magnitudes change as a function of energy. This energy dependence is proportional to $(\alpha^2 + k^2)^{1/2}$ for $^1S_0$ [16], where $\alpha = 0.1$ fm^{-1} is the final-state interaction factor. For $^3P_0$ and $^3P_1$, information from the wave functions directly was used. It was assumed that an average over 1 to 10 MeV captured the significant energy interval for the reaction. Combining the relevant factors results in overlaps of 0.21 for $^1S_0$, 0.9 and 1.2 for $n = 0$ and 1, respectively, for $^3P_0$, and 1.5 and 2.1, respectively, for $n = 0$ and 1 for $^3P_1$.

TABLE II. Partial-wave amplitudes.

J^π	Initial state(s)	Final state	II'	Amplitude(s)
0^-	$^3P_0$	$^1S_0 s$	1 1	f_1
0^+	$^1S_0$	$^3P_0 s$	1 1	f_7
1^-	$^3P_1$	$^3P_0 p$	1 1	f_6
2^-	$^3P_2$, $^3F_2$	$^1S_0 d$	1 1	f_4, f_5
1^+	$^3S_1$, $^3D_1$	$^1S_0 p$	0 1	f_2, f_3

C. Effective $pn \to pp\pi^-$ reaction amplitudes

The final-state $pp\pi^-$ configurations ($^{2S+1}L_J l_\pi$) that enter the σ_{01} cross section are $^1S_0 p$, $^3P_1 s$, $^3P_2 s$, $^3P_0 p, \ldots$; for σ_{11} they are $^1S_0 s$, $^1S_0 d$, $^3P_0 s$, $^3P_0 p$, $^3P_0 d, \ldots$. Here L and J specify the orbital and total angular momentum of the pp pair, respectively, and l_π is the pion angular momentum. The different final-state spectroscopic designations Ss, Ps, Pp, etc., are often referred to as transition classes. For practical reasons of implementation we restrict consideration to the limited number of partial waves listed in Table II, where $L + l_\pi \leqslant 2$. Furthermore, only values of $J = 0$ were included. This is justified by the fact that the terms $^3P_1$ and $^3P_2$ produce the same shapes for the analyzing power and cross-section distributions as for $^3P_0$ (for corresponding values of l_π) in the model. Hence they can effectively be absorbed into the $^3P_0$ amplitude with concomitant effects for the overall value of this amplitude. Indeed, the $^3P_0 s$ and $^3P_0 p$ partial-wave amplitudes contributed negligibly to most of the ^{13}C$(\vec{p}, \pi^-)^{14}$O final states. However, the $^1S_0 d$ partial wave is very important. The last column in Table II is (arbitrarily) assigned the amplitude label indicated.

As detailed below, partial cross sections for the Ss (f_1), Ps (f_7), and Pp (f_6) σ_{11} components were obtained from the $pp \to pp\pi^0$ cross-section measurements. The $pn \to pp(^1S_0)\pi^-$ experiment provided amplitudes and phases for the Ss (f_1) and Sd (f_4,f_5) components of σ_{11} and the Sp (f_2,f_3) components of σ_{01}. The point in common between the two measurements, namely, Ss, provides the normalization for the latter amplitudes and phases. However, there remains much uncertainty for the Sd and Sp amplitudes, given the manner of their determination. No phase information for f_6 and f_7 is available.

Partial cross sections σ_{11} for the $pp \to pp\pi^0$ reaction were obtained from Refs. [6,7], using the division into Ss, Ps, and Pp contributions from Ref. [8]. Within the range of interest, $0.75 \leqslant \eta \leqslant 0.95$, where η is the maximum pion momentum in the three-body final state divided by the pion mass, these can be parameterized approximately as follows:

$$\sigma_{11}(Ss) = 10.7 - 147.0(\eta - 0.85)^2\ \mu\text{b},$$
$$\sigma_{11}(Ps) = 21.1(\eta/0.9)^6\ \mu\text{b}, \quad \sigma_{11}(Pp) = 37.5(\eta/0.9)^6\ \mu\text{b}. \tag{6}$$

These cross sections, when multiplied by the factor 1/2 (see Table I), yield the relevant $pn \to pp\pi^-$ cross sections for σ_{11}. Amplitude f_6 in Table II is assigned the maximum value allowed by $\sigma_{11}(Pp)$, and amplitude f_7 the maximum value allowed by $\sigma_{11}(Ps)$, although, as shown in Ref. [6], the Pp

strength is split over numerous partial waves and so is Ps. It was argued above that these could be meaningfully absorbed into the ^3P_0p and ^3P_0s amplitudes. The cross section $\sigma_{11}(Sd)$, comprising amplitudes f_4 and f_5, could not be extracted from the measurements for the $pp \to pp\pi^0$ reaction because it is too small. However, it does play an important role when polarization effects are considered, as becomes clear in the analysis of the $pn \to pp\pi^-$ measurements [4,5].

Differential cross sections [4] and analyzing powers [5] have been extracted for the $\vec{p}n \to pp(^1S_0)\pi^-$ reaction from measurements of the quasifree $\vec{p}d \to ppp\pi^-$ reaction. The restriction to the $^1S_0$ final pp state was achieved by limiting the detection of the two protons to low relative energies. In order to make the connection between these differential cross sections and the total cross sections referred to above, phase-space and final-state interaction (FSI) calculations were performed, which yielded the pion spectrum over the full range of the relative pp internal energy. These three body $pp\pi^-$ pion energy spectra show that, for the very low pp relative internal energy of 0 to 1.5 MeV, less than 20% of the total pion spectrum was included within the experimental acceptance. Specifically, the relative factors by which the partial cross sections from these measurements [4,17] had to be multiplied to approximate the full cross section were 6.8, 5.8, and 5.3 for $l_\pi = 0$, 1, and 2, respectively. Using this approach the amplitude f_1 was related to the $\sigma_{11}(Ss)$ total cross section, and the approximate normalizations for f_2–f_5 obtained. Clearly, these large extrapolations give rise to large uncertainties in the latter amplitudes and phases.

The $pn \to pp(^1S_0)\pi^-$ experiment extracted the partial-wave amplitudes for three final energies [4,5], $T_{\text{c.m.}} = 31$, 55, and 70 MeV, corresponding to proton bombarding energies of 353, 403, and 440 MeV, respectively, in the $\vec{p}d \to ppp\pi^-$ reaction. For bombarding energies of ∼200 MeV in the $A(p,\pi^-)B$ reaction the final c.m. kinetic energies typically fall between 32 and 48 MeV. Initially attempts were made to derive appropriate energy-dependent amplitudes for the range of interest. Table III, lines (a) and (b), give the amplitudes for $T_{\text{c.m.}} = 48$ and 34 MeV, respectively, as obtained from the original amplitude data derived by Walden [18] and modified using the normalization factors as described above. The corresponding calculated angular distributions of the analyzing powers and differential cross sections are shown in Figs. 2(a) and 2(b) by the solid lines. The dashed lines are obtained using the original unmodified amplitude data [18] (prior to multiplying by the factors 6.8, 5.8, and 5.3). The slight difference in the shapes of the curves arises because of the slightly different weightings of the partial waves and

TABLE III. Complex amplitudes f_1–f_5 $(\text{nb/sr})^{1/2}$.

Line	f_1	f_2	f_3	f_4	f_5
(a)	(132.8,0.0)	(74.7,24.1)	(−82.4,21.7)	(4.8,6.9)	(−7.7,4.8)
(b)	(143.9,0.0)	(58.6,23.2)	(−77.1,14.6)	(−5.5,4.4)	(−3.1,7.2)
(c)	(138.0,0.0)	(43.3,23.3)	(−82.5,23.6)	(−9.4,9.3)	(−13.5,33.6)
(d)	(138.0,0.0)	(0.0,0.0)	(0.0,0.0)	(−9.4,9.3)	(−13.5,33.6)

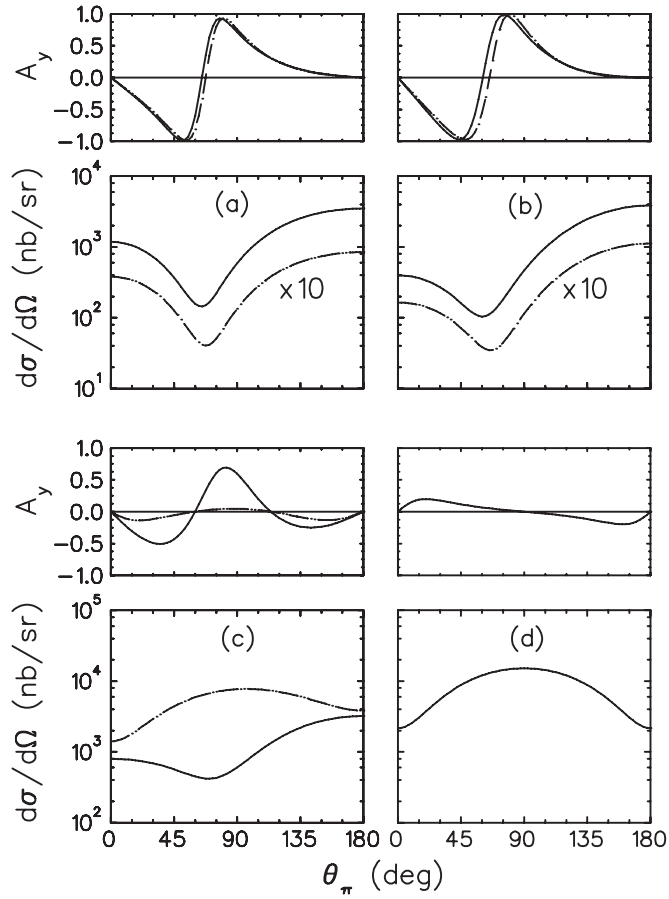

FIG. 2. Analyzing powers and cross sections for the $pn \to pp\pi^-$ reaction. Solid lines in (a)–(c) correspond to the amplitude sets in lines (a)–(c) in Table III ($^1S_0$ protons only). Dashed lines in (a) and (b) are described in the text. The dashed line in (c) was obtained by adding $^3P_0$ amplitudes. (d) A $pp \to pp\pi^0$ simulation described in the text.

serves merely to confirm that these shapes are stable against small relative variations of these amplitudes.

Efforts to use energy-dependent amplitudes proved rather difficult because of the limited information available and also the many additional degrees of freedom introduced. As a result, an averaged set of amplitudes was sought that provided reasonable fits to the $A(p,\pi^-)B$ reaction data. Furthermore, it is expected that within the nuclear environment of the $A(p,\pi^-)B$ reaction these amplitudes will undergo considerable modification from their on-shell values. Consequently, the amplitudes and phases for f_1–f_5 as given in lines (a) and (b) in Table III were treated as starting values only. A modified set of amplitudes is given in line (c) of Table III, and the corresponding calculated distributions in Fig. 2(c) (solid line). Note that this represents a strong enhancement of the pion d-wave amplitudes (f_4 and f_5).

The magnitudes of the partial-wave amplitudes f_6 and f_7 were initially deduced to have values of 131 and 171 $(\text{nb/sr})^{1/2}$, respectively, and, as noted, no phase information was available. In subsequent calculations of $A(p,\pi^-)B$ reactions these were eventually modified to take on values of $f_6 = (-45, 0)$ and $f_7 = (39, 0)$. However, because the role of $^3P_0$ was generally quite weak, except in the case of the 1^- state, much uncertainty

is attached to these values. Also, it will be recalled that the roles of $^3P_1$ and $^3P_2$ were subsumed into $^3P_0$. Nevertheless, the inclusion of $^3P_0$ partial-wave amplitudes in the elementary $pn \to pp\pi^-$ reaction is very important, as shown by the dashed line in Fig. 2(c). However, because of the much smaller contribution of $^3P_0$ in the nuclear case, the dramatic change in the analyzing powers is not observed here.

Finally, a simulation of the $pp \to pp\pi^0$ reaction is obtained by using the amplitudes in line (d) in Table III and the $^3P_0$ amplitudes as previously defined. It is to be noted that there remains considerable uncertainty [8,19,20] with respect to the anisotropy of the pion angular distribution (and hence also the analyzing power). Much of this uncertainty arises from the varying coverage of the pp relative momentum in the various experiments.

D. Transition probabilities and nuclear wave functions

The two-nucleon two-step process envisaged in the models of pion production imply a more restricted set of nuclear transition possibilities for π^- production than for π^+ production. This is so because, in π^- production, the incoming proton interacts with a neutron of the target and returns two protons to previously unfilled states. For π^+ production, on the other hand, the incoming proton interacts with a target proton and returns a neutron and proton to form the final nuclear state. The target proton can originate from a deep-lying state (as well as from a higher-lying state), as the returned proton can refill the deep-lying hole. Thus, in general, there are more transition possibilities for the (p,π^+) reaction than for the (p,π^-) reaction. Nevertheless, in some respects π^+ production may be less complicated, as the isospin of the intermediate core nucleus is restricted to have the isospin of the final nuclear state. This results from the fact that the transferred deuteron has $T = 0$. Indeed, as described below, we include all possibilities of the ^{12}C* core in the states 0.0 MeV, $0^+;0$; 4.44 MeV, $2^+;0$; 12.71 MeV, $1^+;0$; 15.11 MeV, $1^+;1$; and 16.11 MeV, $2^+;1$. All these states are strongly excited in neutron pickup reactions on ^{13}C [21–23].

As indicated in Table II, the two protons transferred to the ^{12}C* core can be in either the $^1S_0$ or the $^3P_0$ configuration. If the former, then the total angular momentum transfer (J_t) of the pair to the core is equal to the orbital angular momentum transfer (L_t). On the other hand, if the protons are in the $^3P_0$ configuration, then $L_t = J_t$ is not allowed; rather, $L_t = J_t \pm 1$.

The model used to obtain the wave functions for the ^{12}C core, ^{14}O, and two-particle parentage amplitudes was the $(0+2)\hbar\omega$ shell model, using the WBT interaction of Warburton and Brown [24]. The OXBASH code [25] was used to obtain the shell-model wave function and two-body parentage amplitudes. The latter are defined as

$$S_{j_1 j_2 J} = \langle J_f \| \left[a^\dagger_{j_2} \times a^\dagger_{j_1}\right]^J \| J_i \rangle, \tag{7}$$

where J_i and J_f are the states in ^{12}C and ^{14}O, respectively. The isospin transfer is taken as $\Delta T = 1$. The $(0+2)\hbar\omega$ space was chosen as that is the minimal space by which two protons may be added to the core and allow significant overlaps, particularly in the sd shell, to be obtained; the two-proton parentage amplitude for the $0\hbar\omega$ model space is trivial.

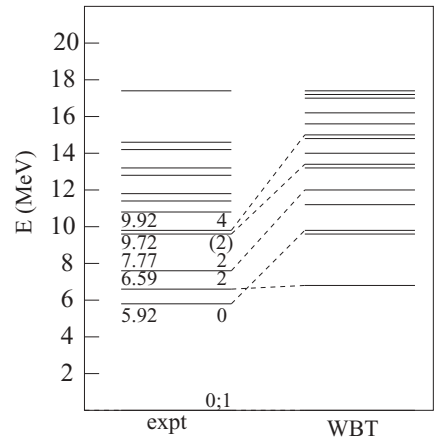

FIG. 3. The ^{14}O spectrum. Experimental results are from Ref. [27].

The model is a reasonable one for ^{12}C, as it reasonably describes all states up to 20 MeV, with the notable exception of the Hoyle state [26]. (The results in Ref. [26] were obtained using the MK3W interaction, which is based on the Cohen and Kurath interactions. The results from the present calculation are largely equivalent.) The results for ^{14}O are shown in Fig. 3, in comparison to data. For the most part, the agreement is reasonable, with most states within 2 MeV of the data.

The two-particle parentage amplitudes, Eq. (7), were obtained for the coupling from the four-core states in ^{12}C listed above to the states with $J_f = 0, 1, 2, 4$ in ^{14}O. To give an example, consider the amplitudes coupling the proton pair to the $2^+_1;0$ state in ^{12}C to give the 2^+_1 state in ^{14}O. The wave function of the ^{12}C state in the $(0+2)\hbar\omega$ model is

$$|2^+_1;0\rangle = 21.39\%|(0p_{3/2})^5(0p_{1/2})^3\rangle + 18.78\% \times |(0p_{3/2})^6(0p_{1/2})^2\rangle + 40.06\%|(0p_{3/2})^7(0p_{1/2})\rangle, \tag{8}$$

with smaller components (<5%) corresponding to configurations with particles in the higher shells. The wave function for the 2^+_1 state in ^{14}O is

$$|2^+_1\rangle = 74.24\%|(0p_{3/2})^7(0p_{1/2})^3\rangle + 6.03\%|(0p_{3/2})^6(0p_{1/2})^2 \times (0d_{5/2})(0d_{3/2})\rangle + 5.08\%|(0p_{3/2})^6(0p_{1/2})^4\rangle, \tag{9}$$

with smaller components (<5%) also with particles in the sd shell. The corresponding amplitudes are dominantly with the proton pair in the $0p$ shell, with intermediate coupling of $J = 0, 2$, as reflected in the wave function for the final state.

A different case is that for the coupling to the 2^+_2 state in ^{14}O. That wave function is predominantly

$$\begin{aligned}|2^+_2\rangle = {} & 22.15\%|(0p_{3/2})^8(0d_{5/2})(1s_{1/2})\rangle \\ & + 19.97\%|(0p_{3/2})^6(0p_{1/2})^2 0d_{5/2} 1s_{1/2}\rangle \\ & + 11.85\%|(0p_{3/2})^6(0p_{1/2})^2(0d_{5/2})^2\rangle \\ & + 9.39\%|(0p_{3/2})^8(0d_{5/2})^2\rangle,\end{aligned} \tag{10}$$

and the amplitudes show significant coupling via a $(0d_{5/2})^2$ proton pair coupled to $J = 0, 2$.

III. RESULTS

A. Remarks on the experimental $^{13}C(\vec{p},\pi^-)^{14}O$ reaction data

In light of a recent study of the excitation energies and level widths of ^{14}O by Negret *et al.* [28], some remarks on the experimental $^{13}C(\vec{p},\pi^-)^{14}O$ data are in order. Those measurements were carried out using the $^{14}N(^3He,t)^{14}O$ reaction, with an experimental resolution of 33 keV (FWHM), while in the $(\vec{p},\pi^-)$ measurements the resolution observed was typically 180 keV [1]. Korkmaz *et al.* [1] assign a spin parity of 2^- to a state at 6.79 MeV. In the earlier literature [27] this state appears 200 keV above the 6.590-MeV 2^+ state. The more recent study [28] gives energy assignments of 6.762 and 6.609 MeV, respectively, and hence a separation of only 153 keV. In addition, the width of 107 keV found for the 6.762-MeV state puts into question the correct separation of these states in the (p,π^-) analysis. Finally, neither Ajzenberg-Selove [27] nor Negret *et al.* [28] confirm a 2^- assignment for this state. Similarly, a (2^+) state at 9.715 MeV [27] is found by Negret *et al.* [28] to be at 9.751 MeV with a width of 147 keV and separated by only 164 keV from the 4^+ state at 9.915 MeV. The second (0^+) at 5.92 MeV, while separated by 352 keV from the nearby 6.272-MeV state, is very weak and poorly defined in the $(\vec{p},\pi^-)$ spectrum. For these reasons the (2^-), (2^+), and (0^+) states referred to above are not considered further in our discussion.

Korkmaz *et al.* [1] also make preliminary assignments of 4^- and 5^- to states at 10.89 and 14.15 MeV, respectively. These are based on comparisons with the $^{13}C(\vec{p},\pi^+)^{14}C$ reactions and on several other observations. Numerous two-neutron and two-proton stripping reactions on ^{12}C have been investigated [27,29]. Common to all these studies is the observation of strong excitation of 3^- and 4^+ states at 6.73 and 10.74 MeV in ^{14}C, respectively, and 6.27 and 9.92 MeV in ^{14}O, respectively. Previous shell-model calculations [30,31] indicate that these states have the configurations $(p_{1/2}d_{5/2})_{3^-}$ and $(d^2_{5/2})_{4^+}$ coupled to a ^{12}C 0^+ core. This is confirmed by the present calculation, which is restricted to positive-parity states, but the present calculation also has an almost-equal parentage with the proton pair coupling to $(d^2_{5/2})_{2^+}$. In addition, the stripping reactions [29,32] show significant excitation of a state at 14.9 MeV in ^{14}C and 14.1 MeV in ^{14}O. These excitations correspond closely to the 14.87- and 14.15-MeV states of Korkmaz *et al.* [1], to which they made tentative 5^- assignments.

B. General features of predicted observables

Numerous calculations were performed for various final states beginning with the originally formulated sets of partial-wave amplitudes as represented by lines (a) and (b) in Table III. The resulting analyzing power angular distributions for the states investigated, with few exceptions, show a strong similarity to those in Figs. 2(a) and 2(b) for the elementary $pn \to pp\pi^-$ reaction; i.e., a rapid transition from highly negative values of A_y to highly positive values. However, this is not what is observed in the experimental data [1]. This is illustrated in Fig. 4 for 0^+ and 5^- states. In addition, it is noted that the strong negative excursion in A_y for the 0^+-state data

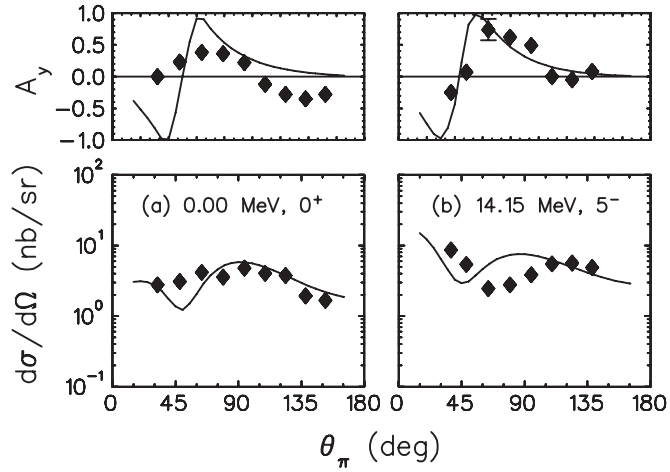

FIG. 4. Calculations for $^{13}C(\vec{p},\pi^-)^{14}O$ for the 0^+ and 5^- states in ^{14}O. The partial wave amplitudes for (a) and (b) correspond to those in lines (a) and (b) of Table III. The data are from Ref. [1]. The calculated cross sections are arbitrarily normalized as shown.

for angles $\geqslant 100^\circ$ is not reproduced in the calculation. The A_y zero-crossing angle of $\sim 55^\circ$ is kinematically shifted to smaller angles in the $A(p,\pi^-)B$ reaction from the $\sim 65^\circ$ value in the elementary reaction in the calculations.

The calculated differential cross sections are typically quite flat, in general agreement with experiment. This outcome can be understood as a combination of the backward peaking of the elementary reaction, as shown in Fig. 2, and the rapid decrease in the reaction matrix element with increasing momentum transfer **q** (or scattering angle). With regard to the magnitudes of the differential cross sections, it is useful to make a comparison with (p,π^+). [The model for the latter reactions typically underestimated the $^{13}C(p,\pi^+)^{14}C$ cross sections by a factor of 2.] The elementary reactions at a bombarding energy of 370 MeV have total cross sections of 550 and 14 μb, respectively, for $pp \to d\pi^+$ and $pn \to pp(^1S_0)\pi^-$. Thus one might expect to find a ratio of ~ 39 for the relative cross sections in the nuclear case. However, because of the small $pn \to pp\pi^-$ cross section at forward angles and the **q** dependence noted above, the ratio in the calculated cross sections would be expected to be considerably higher. Indeed, if the forward angle differential cross sections for the elementary reactions are considered, one finds a ratio of 125. Thus the calculated (p,π^-) cross sections are expected to be about two orders of magnitude smaller than for (p,π^+), a number in rough agreement with the experimental ratio of 75 quoted in Sec. I.

The effect of distortions, treated through eikonal approximations in the model, showed that only the magnitude of the cross sections changed, reducing the latter by $\sim 50\%$. The shapes of the differential cross sections and analyzing powers were essentially identical with and without distortions.

C. Effects of modifications to the partial-wave amplitudes

As noted in the previous section the calculated analyzing powers using the on-shell partial-wave amplitudes produce results that are not consistent with experiment. It is not

unlikely, however, that in the off-shell nuclear process considerable modifications to these partial waves will occur. Consequently, a grid search was made over a range of amplitude and phase for these partial-wave amplitudes. In particular, from the basic model expressions for the analyzing power and the differential cross section, it was apparent that the pion d-wave amplitudes f_4 and f_5 had to be enhanced in order to reproduce the negative A_y at large angles. Much smaller modifications to the pion p-wave amplitudes f_2 and f_3 were found to be adequate. A final compromise set of partial-wave amplitudes for f_1 to f_5 that was used in all the subsequent calculations is indicated on line (c) in Table III. In addition, f_6 and f_7, as previously defined, were used. Calculated results for the $^{13}C(\vec{p}, \pi^-)^{14}O$ reaction using these modified amplitudes are presented in Sec. III E.

D. Sensitivity to nuclear structure effects

The two-proton configurations that couple to the $^{12}C^*$ core to form the final ^{14}O state are quite numerous for each state and, depending on the total angular momentum transfer of the pair and the single-particle states of the protons involved, produce markedly different analyzing powers and differential cross sections. Interference among the contributions of these different two-proton configurations can have a pronounced effect on the observables, especially the magnitude of the cross section. This is illustrated in Fig. 5 for six different configurations that contribute to the population of 0^+ final states in ^{14}O. The designations are $(p)^2_{J_t=0}$, $(p)^2_{J_t=2}$, etc. In addition to the marked differences in the shapes of the analyzing powers and differential cross sections for each configuration, particularly pronounced are the large variations in the cross section magnitudes. For this comparison the strengths of the two-proton configurations were all set to the same value.

It should be mentioned that of all the configurations shown in Fig. 5, only $(p)^2_0$, $(p)^2_2$, and $(d)^2_0$ contribute to the 0^+ ground state. Thus, the particularly strong $(2s)^2_0$ configuration does not contribute.

E. $^{13}C(\vec{p}, \pi^-)^{14}O$ reaction results

Results for the $^{13}C(\vec{p}, \pi^-)^{14}O$ reaction at 200 MeV for eight different states are shown in Figs. 6 and 7. The data are from Korkmaz *et al.* [1]. The calculations used the partial-wave amplitudes given in line (c) of Table III for f_1 to f_5 and the f_6 and f_7 values defined previously. Differential cross sections were arbitrarily normalized to the data as shown. These normalization factors and their significance are discussed below. For the two highest energy states (10.89 and 14.15 MeV) we assume the spin-parity assignments as given in Ref. [1].

The experimental data for the analyzing powers for most of the states $(0^+_1, 1^-_1, 3^-_1, 2^+_1, 5^-_1)$ show rather similar features with marked angular characteristics. These features are generally reproduced in the calculations, except for the extreme forward angles in the first four of these states. On the other hand, the experimental data for the 2^+_2, 4^+_1, and 4^-_1 states exhibit none of these features and are consistent with a constant value over the entire angular range. It is quite possible that cancellation among the nuclear structure terms can produce such a result, but the calculations fail to reproduce them. The error bars for the data for these three states are much larger than for the other states.

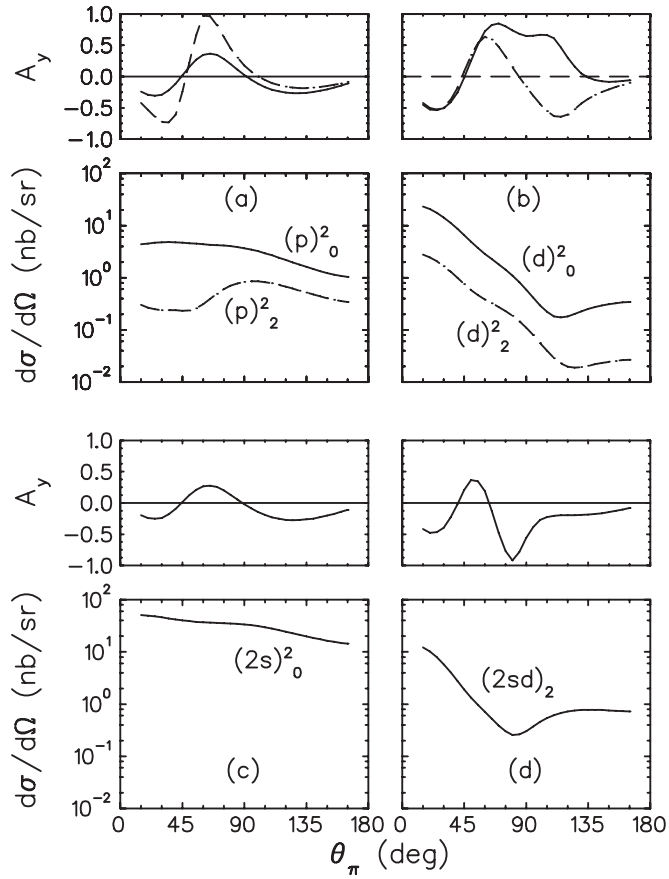

FIG. 5. Sensitivity of observables to the transferred two-proton configurations that contribute to the excitation of 0^+ final states in ^{14}O. The couplings to $J_t = 0$ and 2 correspond to spin values of the $^{12}C^*$ core of 0 and 2, respectively. Partial-wave amplitudes from Table III, line (c), were used.

Very good fits to the angular distributions of the differential cross sections are observed for the 0^+_1, 1^-_1, 3^-_1, and 4^+_1 states, and reasonable fits to the 2^+_1 and 4^-_1 states. As suggested by the results in Fig. 5, the combination of the nuclear structure amplitudes in the transition influences strongly the shapes of the angular distributions of both the differential cross section and the analyzing power.

IV. DISCUSSION

There are many factors which impinge on the magnitude of the cross sections calculated with the current model; a significant one is the nuclear structure amplitudes that enter the calculation. The assumption of a two-step process whereby the initial step produces one of the $^{12}C^*$ core states is also built into the model. Equal population of these core states is assumed. The actual reaction probably does not factor into two parts as simply as assumed. Also significant and deserving of scrutiny are some of the items mentioned in Sec. II. The

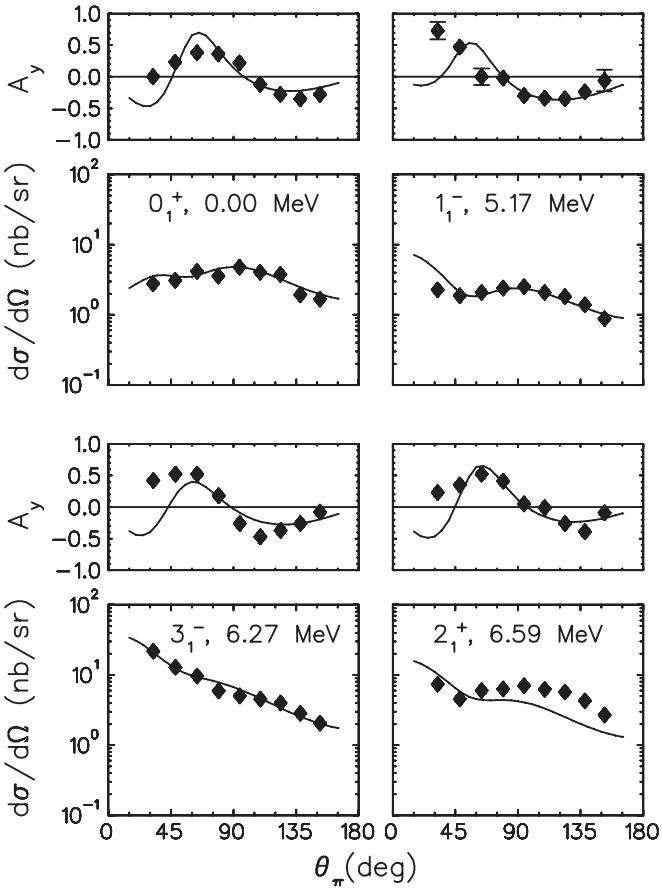

FIG. 6. Results for the $^{13}C(\vec{p},\pi^-)^{14}O$ reaction at 200 MeV. Data are from Ref. [1]. Differential cross sections were arbitrarily normalized to the data as shown.

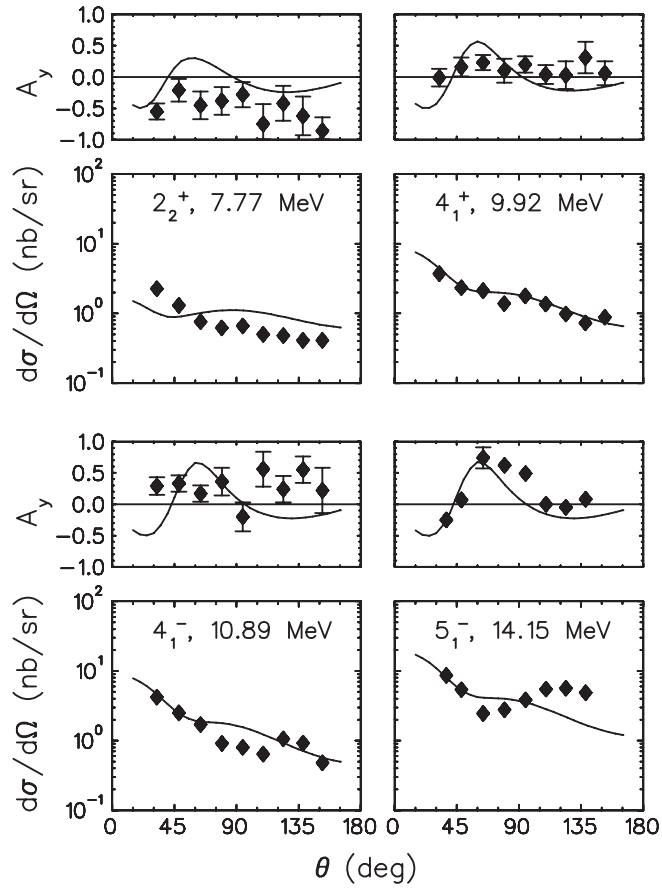

FIG. 7. Results for the $^{13}C(\vec{p},\pi^-)^{14}O$ reaction at 200 MeV. Data are from Ref. [1]. Differential cross sections were arbitrarily normalized to the data as shown.

effective $pn \to pp\pi^-$ cross section for use in the $A(p,\pi^-)B$ reaction, as discussed in Sec. II C, is clearly important. Here we have used the total cross section for this process, which leaves the final protons in the $pp(^1S_0)$ and $pp(^3P_0)$ states. It has been suggested by Kume [11] that higher pp relative angular momentum components [e.g., $pp(^3P_0)$ and others] may well contribute to the $A(p,\pi^-)B$ reaction. In the current study we have found that $pp(^3P_0)$ plays a significant role in only the 1_1^- case. The structure amplitudes for the other states for $pp(^3P_0)$ contribute little. This includes possible $^3P_1$ and $^3P_2$ components which have been subsumed into $^3P_0$. Consequently, the f_6 and f_7 partial waves are poorly determined from this study. Uncertainty in f_2–f_5 arises from the large extrapolation to the full cross section from the very limited acceptance in the $pn \to pp\pi^-$ experiment.

The treatment of the relative motion pp wave function, discussed in Sec. II B, is also open to question. With somewhat different assumptions a change of a factor of 2 or more in the calculated cross sections could easily be obtained. However, this change would affect all states more or less equally.

The attempt to use the free $NN \to NN\pi$ amplitudes in the nuclear environment in the current model may also suffer from the neglect of nuclear correlations. Niskanen and Thomas [33] have shown that in the π^+ absorption on a "deuteron" in ^{3}He a compressed bound state has a marked effect on the cross sections and analyzing powers. In heavier nuclei these effects may be even more pronounced. Likewise, the inclusion of distortions, as treated in the model, affected all states roughly equally, reducing the cross section magnitudes by a factor of 2.

Overall, the model underpredicted the cross-section magnitudes by a factor of about 4 for most states. In the summary of the ratios σ_{exp}/σ_{th} we have first multiplied the model cross sections by this factor, to better display the relative values. These adjusted values σ_{exp}/σ_{th} are shown in Table IV. It should be recalled that the quantity, [overlap of Eq. (5) times the partial

TABLE IV. Differential cross-section normalizations.

State	E_{exc} (MeV)	σ_{exp}/σ_{th}
0_1^+	0.00	10.7
1_1^-	5.17	0.85
3_1^-	6.27	1.5
2_1^+	6.59	3.4
2_2^+	7.77	0.26
4_1^+	9.92	0.15
4_1^-	10.89	0.43
5_1^-	14.15	0.43

wave amplitude] squared, enters into the cross section. Thus a factor of 2 in the combined product of these terms—quite a likely possibility—can account for this factor of 4 in the cross sections.

Excluding the 0_1^+ state, which clearly is an outlier, the remaining ratios still vary considerably. For 0_1^+ it was noted earlier that, among the structure amplitudes for this state, the strong $(2s)_0^2$ two-proton configuration (see Fig. 5) was absent. Some admixture of this component could alter this ratio considerably.

V. CONCLUSION

A phenomenological model of $A(\vec{p},\pi^-)B$ reactions has been presented that incorporates the experimental data on the $\vec{p}n \to pp\pi^-$ reaction. The model, applied extensively to numerous final states in the $^{13}C(\vec{p},\pi^-)^{14}O$ reaction, shows broad agreement with the data on the shapes of the differential cross sections but predicts strengths which vary considerably from state to state. A particularly small cross section is predicted for the 0_1^+ state. For such weak states the role of pion charge exchange, as described in Sec. I, may be particularly important. Further studies should investigate the role of such processes.

Calculated analyzing powers have certain common features for many of the states investigated—namely, a negative region for $\theta_\pi \leqslant 45^\circ$, a positive region for $45^\circ \leqslant \theta_\pi \leqslant 90^\circ$, and, again, a negative region for $\theta_\pi \geqslant 90^\circ$. This conforms quite well with the experimental data for those states that exhibit the more typical A_y distribution. For the 2^+, 4^+, and 4^- states in Fig. 7 the atypical analyzing powers are not reproduced.

The use of a single set of amplitudes representing the elementary $\vec{p}n \to pp\pi^-$ reaction—in $^{13}C(\vec{p},\pi^-)^{14}O$ reactions where the pion c.m. energies vary from 48 to 34 MeV—may well be questioned. On the other hand, the many degrees of freedom available without this constraint made any general deductions too difficult. While an optimum set of amplitudes could often be found for a particular state that provided a good fit to the differential cross section or the analyzing power, such a set would generally not be suitable for all the other states.

Future investigations of $A(\vec{p},\pi^-)B$ reactions must clarify the role of nuclear structure effects, nuclear correlations, distortions, dynamical effects, possible pion charge exchange effects, and particulars of the $\vec{p}n \to pp\pi^-$ process itself. The phenomenological model described in this paper, while capturing many of the experimental features of the reaction, is not adequate to describe all the facets of this complicated reaction.

ACKNOWLEDGMENT

One of us (S.K.) acknowledges support from the National Research Foundation of South Africa.

[1] E. Korkmaz *et al.*, Phys. Rev. C **40**, 813 (1989).
[2] W. R. Falk, Phys. Rev. C **50**, 1574 (1994).
[3] W. R. Falk, Phys. Rev. C **61**, 034005 (2000).
[4] F. Duncan *et al.*, Phys. Rev. Lett. **80**, 4390 (1998).
[5] H. Hahn *et al.*, Phys. Rev. Lett. **82**, 2258 (1999).
[6] H. O. Meyer *et al.*, Phys. Rev. C **63**, 064002 (2001).
[7] R. Bilger *et al.*, Nucl. Phys. A **693**, 663 (2001).
[8] S. A. El-Samad *et al.*, Eur. Phys. J. A **17**, 595 (2003).
[9] W. W. Jacobs, T. G. Throwe, S. E. Vigdor, M. C. Green, J. R. Hall, H. O. Meyer, W. K. Pitts, and M. Dillig, Phys. Rev. Lett. **49**, 855 (1982).
[10] N. Nose-Togawa, K. Kume, and H. Toki, Phys. Rev. C **57**, 2502 (1998), and references therein.
[11] K. Kume, Phys. Lett. B **57**, 17 (1991).
[12] N. Nose, K. Kume, and H. Toki, Phys. Rev. C **53**, 2324 (1996).
[13] K. Kume and N. Nose, Nucl. Phys. A **528**, 723 (1991).
[14] N. Nose and K. Kume, Phys. Rev. C **45**, 2879 (1992).
[15] B. Loiseau and L. Mathelitsch, Z. Phys. A **358**, 435 (1997); B. Loiseau (private communication).
[16] G. Fäldt and C. Wilkin, Phys. Lett. B **382**, 209 (1996); M. L. Goldhaber and K. M. Watson, *Collision Theory* (John Wiley and Sons, New York, 1964).
[17] F. A. Duncan, Ph.D. thesis, University of British Columbia, 1993 (unpublished).
[18] P. Walden (private communication).
[19] P. Thörngren Engblom *et al.*, Phys. Rev. C **76**, 011602 (2007).
[20] Y. Maeda *et al.*, Phys. Rev. C **77**, 044004 (2008).
[21] R. P. Liljestrand *et al.*, Phys. Lett. B **99**, 311 (1981).
[22] J. D. Cossairt and D. P. May, Nucl. Phys. A **319**, 182 (1979).
[23] K. Kosono *et al.*, Nucl. Phys. A **343**, 234 (1980).
[24] E. K. Warburton and B. A. Brown, Phys. Rev. C **46**, 923 (1992).
[25] A. Etchegoyen, W. D. M. Rae, and N. S. Godwin, OXBASH-MSU (Oxford-Buenos-Aires-Michigan State University shell model code) (MSU version by B. A. Brown, 1986); B. A. Brown, A. Etchegoyen, and W. D. M. Rae, MSUCL Report No. 524, unpublished (1986).
[26] S. Karataglidis, P. J. Dortmans, K. Amos, and R. de Swiniarski, Phys. Rev. C **52**, 861 (1995).
[27] F. Ajzenberg-Selove, Nucl. Phys. A **523**, 1 (1991).
[28] A. Negret *et al.*, Phys. Rev. C **71**, 047303 (2005).
[29] L. Kraus *et al.*, Phys. Rev. C **37**, 2529 (1988), and references cited therein.
[30] S. Lie, Nucl. Phys. A **181**, 517 (1972).
[31] A. Boucenna, Nuovo Cimento A **110**, 711 (1997).
[32] R. Jahn, D. P. Stahel, G. J. Wozniak, R. J. de Meijer, and J. Cerny, Phys. Rev. C **18**, 9 (1978).
[33] J. A. Niskanen and A. W. Thomas, Phys. Lett. B **196**, 299 (1987).